International Journal of Multiphase Flow 36 (2010) 847–857

Contents lists available at ScienceDirect

International Journal of Multiphase Flow

journal homepage: www.elsevier.com/locate/ijmulflow

Effects of inertia and surface tension on a power-law fluid flowing down a wavy incline

C. Heining *, N. Aksel

Applied Mechanics and Fluid Dynamics, University of Bayreuth, D-95440 Bayreuth, Germany

ARTICLE INFO

Article history:
Received 12 April 2010
Received in revised form 17 June 2010
Accepted 16 July 2010
Available online 24 July 2010

Keywords:
Film flow over topography
Power-law liquid
Linear and nonlinear stability
Surface tension

ABSTRACT

We consider a thin film of a power-law liquid flowing down an inclined wall with sinusoidal topography. Based on the von Kármán–Pohlhausen method an integral boundary-layer model for the film thickness and the flow rate is derived. This allows us to study the influence of the non-Newtonian properties on the steady free surface deformation. For weakly undulated walls we solve the governing equation analytically by a perturbation approach and find a resonant interaction of the free surface with the wavy bottom. Furthermore, the analytical approximation is validated by numerical simulations. Increasing the steepness of the wall reveals that nonlinear effects like the resonance of higher harmonics grow in importance. We find that shear-thickening flows lead to a decrease while shear thinning flows lead to an amplification of the steady free surface. A linear stability analysis of the steady state shows that the bottom undulation has in most cases a stabilizing influence on the free surface. Shear thickening fluids enhance this effect. The open questions which occurred in the linear analysis are then clarified by a nonlinear stability analysis. Finally, we show the important role of capillarity and discuss its influence on the steady solution and on the stability.

1. Introduction

The steady, unidirectional gravity-driven flow of a Newtonian liquid over a flat incline is a fundamental problem in fluid mechanics which has even an exact analytical solution. However, many applications in environmental (Hutter et al., 1996; Fowler, 1982) and industrial systems (Kistler and Schweizer, 1997) require more complex geometries such as bottom corrugations (Argyriadi et al., 2006), undulations (Wierschem et al., 2005) or complex liquids with non-Newtonian behaviour (Lawrence and Zhou, 1991). Bottom corrugations may considerably affect the heat- and mass transfer in heat and mass exchangers (Kanaris and Mouza, 2006) and non-Newtonian flows encounter for example in coating systems and in the modeling of debris, lava or glacier flow.

Although the steady base problem of a Newtonian liquid flowing over an even substrate has a simple analytical solution, the extension to other systems mostly requires to model the whole set of equations including the free surface which is not known a priori but comes out as part of the solution. Starting with the pioneering work of Shkadov (1967) who applied the integral boundary-layer theory to a thin film flow of a viscous liquid along a flat wall, many other researches adopted his idea to more complex geometries or complex fluids. Trifonov (1998) extended the theory to the flow over an undulated topography and Oron and Heining (2008) developed a higher order model based on the ideas of Ruyer-Quil and Manneville (2000). The studies in the literature reveal that the geometry induces surface effects like hydraulic jumps, standing waves (Wierschem and Aksel, 2004a), resonance (Wierschem et al., 2008; Heining et al., 2009) and stabilization of kinematic surface waves (Wierschem and Aksel, 2003; Dávalos-Orozco, 2007, 2008; Trifonov, 2007a,b) and flow field effects like the generation of eddies (Wierschem et al., 2003; Scholle et al., 2004, 2009; Wierschem and Aksel, 2004b) which are impossible in the flow over flat inclines.

Other researchers focused on the flow and the instability of non-Newtonian films along flat inclines, among them Gupta (1967) for a second order fluid and Berezin et al. (1998) for a power-law fluid. Dandapat and Mukhopadhyay (2001) studied surface waves of a falling power-law fluid in the integral boundary-layer framework, while Miladinova et al. (2004) considered the same problem in the lubrication approximation. Recently, Amaouche et al. (2009) developed an extension of the model equations of Ruyer-Quil and Manneville (2000) which correctly predict the linear stability threshold. Other effects studied in literature are the influence of surfactants (Pozrikidis, 2003), electric fields (Tseluiko et al., 2008), porosity (Pascal, 2006; Sadiq and Usha, 2008; Pascal and D'Alessio, 2010), external stresses (Pascal, 2003; Pascal and D'Alessio, 2007), three-dimensionality (Luo and Pozrikidis, 2007) and evaporation (Gaskell et al., 2006) on thin film flow to name a

* Tel.: +49 921557262; fax: +49 921557265.
E-mail address: christian.heining@uni-bayreuth.de (C. Heining).

0301-9322/$ - see front matter © 2010 Elsevier Ltd. All rights reserved.
doi:10.1016/j.ijmultiphaseflow.2010.07.002

few. An overview over further effects is provided in Craster and Matar (2009).

Saprykin et al. (2007) studied inertial effects on the flow of a viscoelastic liquid over a step-down topography. Nevertheless, the influence of a wavy wall on the steady film and its stability for a non-Newtonian fluid has not been studied yet and will be provided by the present work. The outline is as follows: First, the governing equations are derived in Section 2. In Section 3, we solve the steady integral boundary-layer model analytically for weak undulations and numerically for arbitrary undulations; we find conditions for maximum amplification of the free surface and study the influence of the power-law index on the free surface. The numerical simulations allow us to compare the results with the analytical predictions. In Section 4, we study the linear and nonlinear stability of the steady solutions and determine the critical Reynolds number for the onset of surface waves, depending on the undulation and the power-law index. In Section 5, the role of surface tension and its impact on the steady film and the stability is clarified. Finally, the results and conclusions are discussed in Section 6.

2. Derivation of the governing equations

We study an incompressible power-law liquid in the gravity field $\vec{g}$ flowing down an inclined undulated substrate at inclination angle α. The contour of the topography is given by the periodic function $b(x) = a\cos(2\pi x/\lambda)$, where x is the coordinate in the mean flow direction, a the amplitude of the undulation and λ its wavelength, respectively. The coordinate perpendicular to the x -axis is denoted by y. We give an overview of the problem setup in Fig. 1. We note that the flow direction in this and in all following figures showing free surface profiles is from the left to the right. The stress tensor τ_{ij} of the liquid is defined by (Spurk and Aksel, 2008)

$$\tau_{ij} = 2\eta_n (2D_{kl}D_{kl})^{(n-1)/2} D_{ij}, \tag{1}$$

where

$$D_{ij} = \frac{1}{2}\left(\frac{\partial u_i}{\partial x_j} + \frac{\partial u_j}{\partial x_i}\right) \tag{2}$$

denotes the strain-rate tensor with the velocities u_i and spatial variables x_i. In Eqs. (1) and (2) the sum convention is employed. The constants η_n and n are material properties: The constant η_n with the dimension $[\eta_n] = kgm^{-1}s^{n-2}$ is the so-called consistency factor of the liquid, a higher η_n indicates a more 'viscous' liquid and n measures the departure from the Newtonian behaviour (Aksel and Heymann, 2007). Obviously, in the case $n = 1$ Eq. (1) reduces to the Newtonian case. For $n < 1$ the fluid is shear-thinning and for $n > 1$ shear-thickening. We note that power-law fluids serve as a simple but an efficient model for a broad variety of non-Newtonian fluids like miscellar solutions (Teipel et al., 2001), suspensions and emulsions (Aksel and Heymann, 2007) and even for biological cells (Fernandez et al., 2007). For further details we refer to Aksel and Heymann (2007). The other fluid properties, apart from the non-Newtonian behaviour, are density and surface tension, denoted by ρ and σ, respectively.

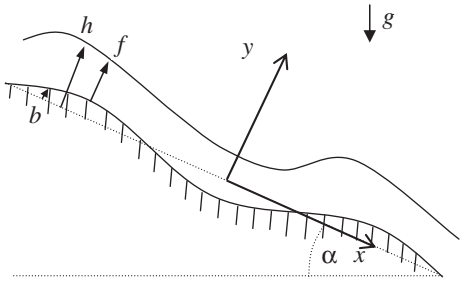

Fig. 1. Flow of a power-law liquid down an incline with inclination angle α. Driving force is gravity g. In the (x, y) – coordinate system the film thickness, free surface position and topography are denoted by f, h and b, respectively.

The steady flow over a flat incline shows a constant free surface position $y = d$. In the presence of an unsteady flow over an undulated wall the interplay of the fluid between the substrate and gravity causes an unknown free surface deformation which is denoted by $h(x, t)$. The film thickness distribution $f(x, t)$ is then given by the relation $h(x, t) = b(x) + f(x, t)$. Furthermore, we have three unknown flow variables, namely the velocities u, v and the pressure p which all depend on the spatial variables x, y and the time t.

The mass and momentum balance read

$$\begin{aligned}
&\tfrac{\partial u}{\partial x} + \tfrac{\partial v}{\partial y} = 0,\\
&\rho\left(\tfrac{\partial u}{\partial t} + u\tfrac{\partial u}{\partial x} + v\tfrac{\partial u}{\partial y}\right) = -\tfrac{\partial p}{\partial x} + \rho g\sin\alpha + \tfrac{\partial \tau_{xx}}{\partial x} + \tfrac{\partial \tau_{xy}}{\partial y},\\
&\rho\left(\tfrac{\partial v}{\partial t} + u\tfrac{\partial v}{\partial x} + v\tfrac{\partial v}{\partial y}\right) = -\tfrac{\partial p}{\partial y} - \rho g\cos\alpha + \tfrac{\partial \tau_{yx}}{\partial x} + \tfrac{\partial \tau_{yy}}{\partial y}.
\end{aligned} \tag{3}$$

The field equations are complemented by the no-slip and no-penetration condition at the substrate $y = b(x)$

$$u = v = 0, \tag{4}$$

and the kinematic boundary condition and the two components of the dynamic boundary condition at the free surface $y = h(x, t)$:

$$\begin{aligned}
&\tfrac{\partial h}{\partial t} + u\tfrac{\partial h}{\partial x} = v,\\
&\tau_{yx}\left(1 - \left(\tfrac{\partial h}{\partial x}\right)^2\right) - (\tau_{xx} - \tau_{yy})\tfrac{\partial h}{\partial x} = 0,\\
&p - p_{air} = -\sigma\tfrac{\partial^2 h}{\partial x^2}\left(1 + \left(\tfrac{\partial h}{\partial x}\right)^2\right)^{-3/2}\\
&\qquad + \left(\tau_{xx}\left(\tfrac{\partial h}{\partial x}\right)^2 - 2\tau_{yx}\tfrac{\partial h}{\partial x} + \tau_{yy}\right)\left(1 + \left(\tfrac{\partial h}{\partial x}\right)^2\right)^{-1},
\end{aligned} \tag{5}$$

where p_{air} denotes the passive gas over the fluid film.

The correspondence to the flow over a flat incline motivates us to adopt the scaling in Miladinova et al. (2004). In the case of the flow over a flat incline the steady velocity reads

$$u = \frac{n}{1+n}\left(\frac{\rho g\sin\alpha}{\eta_n}\right)^{1/n} d^{(1+n)/n}\left[1 - \left(1 - \frac{y}{d}\right)^{(1+n)/n}\right]. \tag{6}$$

It has to be noted that the other velocity component vanishes: $v = 0$. The solution (6) can be obtained by solving the steady momentum balance under the assumption of an unidirectional flow. As characteristic scales we choose

$$\begin{aligned}
&x = \frac{\lambda}{2\pi}x^* \quad y = dy^* \quad f = df^*\\
&h = dh^* \quad b = ab^* \quad p = \rho\bar{u}^2 p^*\\
&u = \bar{u}u^* \quad v = \frac{2\pi d}{\lambda}\bar{u}v^* \quad t = \frac{\lambda}{2\pi\bar{u}}t^*\\
&\tau = \eta_n\frac{\bar{u}^n}{d^n}\tau^*,
\end{aligned} \tag{7}$$

where $\bar{u}$ is the mean velocity of the Nusselt film given by the relation

$$\bar{u} = \frac{1}{d}\int_0^d u(y)dy = \frac{n}{1+2n}\left(\frac{\rho g\sin\alpha}{\eta_n}\right)^{1/n} d^{(1+n)/n}. \tag{8}$$

We remark that the dimensional reference flow rate is defined by the expression $q = \bar{u}d$. The quantities in (7) with asterisk denote dimensionless variables. In the following the asterisk is omitted and all field equations are dimensionless. In dimensionless form the constitutive equation reads

$$\tau_{ij} = 2\left[2\delta^2\left(\left(\frac{\partial u}{\partial x}\right)^2 + \left(\frac{\partial v}{\partial y}\right)^2\right) + \left(\delta^2\frac{\partial v}{\partial x} + \frac{\partial u}{\partial y}\right)^2\right]^{\frac{n-1}{2}} \times \begin{pmatrix} \delta\frac{\partial u}{\partial x} & \frac{1}{2}\left(\delta^2\frac{\partial v}{\partial x} + \frac{\partial u}{\partial y}\right) \\ \frac{1}{2}\left(\delta^2\frac{\partial v}{\partial x} + \frac{\partial u}{\partial y}\right) & \delta\frac{\partial v}{\partial y} \end{pmatrix}, \tag{9}$$

where we introduced the dimensionless quantity $\delta = 2\pi d/\lambda$, which will be referred to as the dimensionless film thickness parameter. Substituting the scaling (7) into the field equations (3) and boundary conditions (4), (5) we arrive at the dimensionless formulation of the problem. The field equations then read

$$\begin{aligned} \delta\mathrm{Re}\left(\frac{\partial u}{\partial t} + u\frac{\partial u}{\partial x} + v\frac{\partial u}{\partial y}\right) &= -\delta\mathrm{Re}\frac{\partial p}{\partial x} + \left(\frac{n}{1+2n}\right)^{-n} + \delta\frac{\partial \tau_{xx}}{\partial x} + \frac{\partial \tau_{xy}}{\partial y}, \\ \delta^3\mathrm{Re}\left(\frac{\partial v}{\partial t} + u\frac{\partial v}{\partial x} + v\frac{\partial v}{\partial y}\right) &= -\delta\mathrm{Re}\frac{\partial p}{\partial y} - \left(\frac{n}{1+2n}\right)^{-n}\delta\cot\alpha \\ &\quad + \delta^2\frac{\partial \tau_{yx}}{\partial x} + \delta\frac{\partial \tau_{yy}}{\partial y}, \end{aligned} \tag{10}$$

$$\frac{\partial u}{\partial x} + \frac{\partial v}{\partial y} = 0, \tag{11}$$

where we introduced a generalized Reynolds number in line with Dandapat and Mukhopadhyay (2003) defined as

$$\mathrm{Re} = \frac{\rho\bar{u}^{2-n}d^n}{\eta_n}. \tag{12}$$

The form of (12) becomes clear by considering the ratio of the characteristic mass flow rate $\rho\bar{u}d$ to the viscous term given by $\eta_n(\bar{u}^2/d^2)^{(n-1)/2}$, see Eq. (1). The no-slip and no-penetration condition at the substrate $y = \xi b(x)$ remain unchanged $u = v = 0$. As a consequence of our scaling a steepness parameter $\xi = a/d$ enters in the boundary condition measuring the deviation from the case of a flat substrate. For $\xi = 0$ the problem reduces to the system with the solution (6) in dimensional form.

The boundary conditions at the free surface $y = h$ read

$$\frac{\partial h}{\partial t} + u\frac{\partial h}{\partial x} = v, \tag{13}$$

$$\tau_{yx}\left[1 - \delta^2\left(\frac{\partial h}{\partial x}\right)^2\right] - \delta(\tau_{xx} - \tau_{yy})\frac{\partial h}{\partial x} = 0,$$

$$\begin{aligned} \delta\mathrm{Re}(p - p_{air}) &= -3\delta Bo^{-1}\frac{\partial^2 h}{\partial x^2}\left[1 + \delta^2\left(\frac{\partial h}{\partial x}\right)^2\right]^{-3/2} \\ &\quad + \left[\delta^3\tau_{xx}\left(\frac{\partial h}{\partial x}\right)^2 - 2\delta^2\tau_{yx}\frac{\partial h}{\partial x} + \delta\tau_{yy}\right]\left[1 + \delta^2\left(\frac{\partial h}{\partial x}\right)^2\right]^{-1}, \end{aligned} \tag{14}$$

where the generalized inverse Bond number has been introduced as a measure for surface tension σ. In analogy to the generalized Reynolds number, the generalized inverse Bond number is defined as $Bo^{-1} = (1/3)((1+2n)/n)^n \cdot (2\pi l_{Ca})^2/(\lambda^2\sin\alpha)$ with the capillary length $l_{Ca} = \sqrt{\sigma/(\rho g)}$. It couples the power-law index with the inverse Bond number for Newtonian flows (Wierschem et al., 2008). To sum it up, the above formulated problem is embedded in a 6-dimensional parameter space with Re, Bo^{-1}, $\cot\alpha$, δ, ξ and n. We remark that other authors use different sets of dimensionless parameters. For example in the case of the non-Newtonian flow over a flat incline (Dandapat and Mukhopadhyay, 2001) or the Newtonian flow over an undulated incline (Trifonov, 2007b) the Kapitza or film number is introduced. This leads to the set of non-dimensional parameters Re, $\lambda/l_{Ca}, a/\lambda, \cot\alpha, n$ and Ka, where $Ka = (\sigma/\rho)^{2+n}g^{2-3n}(\eta_n/\rho)^{-4}$ is the Kapitza number, which has the advantage that only one parameter depends on the flow rate. From the dimensionless point of view both sets are equivalent. Since the present work is an extension of Wierschem et al. (2008) and Heining et al. (2009) we use the same dimensionless parameters here for convenience.

In the following, we assume a thin film approximation (Heining et al., 2009) and truncate equations (10), (14) at order δ^2 assuming that $\delta Re = O(1)$, $\delta\cot\alpha = O(1)$ and $\delta Bo^{-1} = O(1)$. After substituting the stress tensor (9) the leading order momentum balance reads

$$\delta\mathrm{Re}\left(\frac{\partial u}{\partial t} + u\frac{\partial u}{\partial x} + v\frac{\partial u}{\partial y}\right) = -\delta\mathrm{Re}\frac{\partial p}{\partial x} + \left(\frac{n}{1+2n}\right)^{-n} + \frac{\partial}{\partial y}\left(\frac{\partial u}{\partial y}\right)^n, \tag{15}$$

$$0 = -\delta\mathrm{Re}\frac{\partial p}{\partial y} - \left(\frac{n}{1+2n}\right)^{-n}\delta\cot\alpha. \tag{16}$$

The no-slip, no-penetration condition at the substrate $y = \xi b$ and the kinematic boundary condition at the free surface $y = h$ remain still unchanged. After substituting the stress tensor (9) the dynamic boundary condition (14) yields at leading order

$$0 = \frac{\partial u}{\partial y}, \tag{17}$$

$$\delta\mathrm{Re}(p - p_{air}) = -\delta Bo^{-1}\frac{\partial^2 h}{\partial x^2}. \tag{18}$$

Eq. (16) can be integrated and gives, after inserting the dynamic boundary condition (18), an expression for the pressure:

$$\delta\mathrm{Re}p = \delta\mathrm{Re}p_{air} - 3\delta Bo^{-1}\frac{\partial^2 h}{\partial x^2} + \left(\frac{n}{1+2n}\right)^{-n}\delta\cot\alpha(h - y). \tag{19}$$

This expression can then be used to eliminate the pressure in the momentum balance (15) which yields

$$\begin{aligned} \delta\mathrm{Re}\left(\frac{\partial u}{\partial t} + u\frac{\partial u}{\partial x} + v\frac{\partial u}{\partial y}\right) &= 3\delta Bo^{-1}\frac{\partial^3 h}{\partial x^3} \\ &\quad - \left(\frac{n}{1+2n}\right)^{-n}\delta\cot\alpha\frac{\partial h}{\partial x} \\ &\quad + \left(\frac{n}{1+2n}\right)^{-n} + \frac{\partial}{\partial y}\left(\frac{\partial u}{\partial y}\right)^n. \end{aligned} \tag{20}$$

In the following, we apply the Kármán-Pohlhausen integral boundary-layer method (Kármán, 1921; Pohlhausen, 1921) and integrate Eq. (20) with respect to y from the substrate $y = \xi b$ to the free surface $y = h$. After substituting $f = h - \xi b$ the resulting equation reads

$$\begin{aligned} \delta\mathrm{Re}\left(\frac{\partial}{\partial t}\int_{\xi b}^{h} u\,dy + \frac{\partial}{\partial x}\int_{\xi b}^{h} u^2\,dy\right) &= 3\delta Bo^{-1}\frac{\partial^3 h}{\partial x^3}f - \left(\frac{n}{1+2n}\right)^{-n} \\ &\quad \times \delta\cot\alpha\frac{\partial h}{\partial x}f + \left(\frac{n}{1+2n}\right)^{-n}f - \left(\frac{\partial u}{\partial y}\right)^n\Big|_{y=\xi b}, \end{aligned} \tag{21}$$

where we already made use of the no-slip boundary condition, the dynamic boundary condition (17) and applied Leibniz' integration rule. After averaging the continuity equation (11) and applying the kinematic boundary condition (13) we obtain

$$\frac{\partial h}{\partial t} + \frac{\partial q}{\partial x} = 0, \tag{22}$$

where we introduced the flow rate per unit film width

$$q = \int_{\xi b}^{h} u\,dy. \tag{23}$$

The averaging process has the consequence that local information is partially lost. The system given by the integral momentum balance (21) and the integral mass balance (22) contains three unknown variables u, q and h which have to be determined by only two

equations. To close the system, a specific velocity profile has to be introduced. We follow the idea in Heining et al. (2009) and assume that the velocity profile in the case of the flow over a slightly undulated topography is locally close to that of a flat incline. Comparisons with experiments and theoretical investigations have shown that this reflects the reality quite well for Newtonian liquids (Wierschem et al., 2002). We hence take the velocity profile (6) and adopt it to the undulated topography. It then reads in dimensionless form

$$u = \frac{1+2n}{1+n}\frac{q}{f}[1-(1-(y-\xi b)/f)^{(1+n)/n}]. \tag{24}$$

In the case of a Newtonian liquid with $n = 1$ Eq. (24) reduces to a parabolic velocity profile. The other velocity component can be computed by applying the continuity equation but it is not relevant for the following since it has been eliminated in (21).

Substituting the velocity profile (24) into the momentum balance (21), we finally arrive at the integral boundary-layer model, denoted as IBL model in the following:

$$\delta\mathrm{Re}\left(\frac{\partial q}{\partial t}+\frac{2(1+2n)}{2+3n}\frac{\partial}{\partial x}\left(\frac{q^2}{f}\right)\right) = 3\delta Bo^{-1}\frac{\partial^3 h}{\partial x^3}f + \frac{1}{3}\left(\frac{1+2n}{n}\right)^n\left(-3\delta\cot\alpha\frac{\partial h}{\partial x}f+3f-\frac{3q^n}{f^{2n}}\right). \tag{25}$$

In the steady case with $\partial/\partial t = 0$ the continuity equation (22) can be integrated yielding $q = 1$ and the shape of the free surface is completely described by the momentum balance (25). We therefore have to solve an ordinary differential equation for the steady film thickness f.

In this paper, particularly the influence of the steepness parameter ξ and the power-law index n on the response of the free surface will be investigated. In the case of the steady flow over a periodically undulating contour with $b = \cos x$ the IBL-model (25) reads

$$\delta\mathrm{Re}\left(\frac{2(1+2n)}{2+3n}\frac{d}{dx}\left(\frac{1}{f}\right)\right) = 3\delta Bo^{-1}\frac{d^3 f}{dx^3}f + \frac{1}{3}\left(\frac{1+2n}{n}\right)^n\left(-3\delta\cot\alpha\frac{df}{dx}f+3f-\frac{3}{f^{2n}}\right) + \left(3\delta Bo^{-1}+\left(\frac{1+2n}{n}\right)^n\delta\cot\alpha\right)f\xi\sin x. \tag{26}$$

Tracing back the terms in (26) to the original momentum balance allows us to identify their origin: (i) The left hand side is responsible for the influence of inertia. (ii) The first term at the right hand side measures the influence of surface tension and comes into play through the dynamic boundary condition. (iii) The second line of (26) includes the hydrostatic pressure, the gravitational forcing and the wall shear stress. (iv) The periodic inhomogeneity in the last line comes from the forcing due to the undulated topography.

3. Linear and nonlinear resonance of the free surface

In this section, we seek for steady analytical and numerical solutions of the IBL model (26). To begin with, we assume periodic undulations with weak steepness:

$$\xi \ll 1. \tag{27}$$

In this case the solution $f(x)$ can be determined by using ξ as a perturbation parameter and expanding the film thickness into a series in ξ:

$$f = 1 + \xi f_1 + O(\xi^2). \tag{28}$$

In the expansion (28) we already incorporated the information that $f_0 = 1$ in the basic case corresponding to the steady flow over a flat wall. Substituting the expansion (28) into the steady IBL-model (26) yields at order ξ^1

$$0 = \left(3(1-2n)f_1+3\delta\cot a\frac{df_1}{dx}\right)\frac{1}{3}\left(\frac{1+2n}{n}\right)^n - 3\delta Bo^{-1}\frac{d^3 f_1}{dx^3} - \delta\mathrm{Re}\left(\frac{2(1+2n)}{2+3n}\right)\frac{df_1}{dx} - 3\left(\delta Bo^{-1}+\frac{1}{3}\left(\frac{1+2n}{n}\right)^n\delta\cot a\right)\sin x, \tag{29}$$

which is a linear ordinary differential equation for the first order film thickness f_1. According to the periodicity of the inhomogeneity we assume that the solution inherits the periodicity of the substrate and can be written as a periodic function with the same periodicity as the substrate contour, hence

$$f_1 = S_1\sin x + C_1\cos x, \tag{30}$$

with constants S_1, C_1 which have to be determined. Substituting (30) into (29) and equating like coefficients yields the solution

$$S_1 = \frac{-3(1+2n)K_2(3K_2\delta\cot\alpha+3\delta Bo^{-1})}{(3K_2\delta\cot\alpha+3\delta Bo^{-1}-\delta\mathrm{Re}K_1)^2+9K_2^2(1+2n)^2},$$
$$C_1 = \frac{-(3K_2\delta\cot\alpha+3\delta Bo^{-1}-\delta\mathrm{Re}K_1)(3K_2\delta\cot\alpha+3\delta Bo^{-1})}{(3K_2\delta\cot\alpha+3\delta Bo^{-1}-\delta\mathrm{Re}K_1)^2+9K_2^2(1+2n)^2}, \tag{31}$$

where we introduced the abbreviations $K_1 = 2(1+2n)/(2+3n)$ and $K_2 = ((1+2n)/n)^n/3$ which only depend on the power-law index n.

We are now able to study the impact of n on the free surface deformation by considering the solution up to first order in ξ

$$f = 1 + \xi(S_1\sin x + C_1\cos x). \tag{32}$$

The free surface position at first order then reads $h = \xi\cos x + 1 + \xi(S_1\sin x + C_1\cos x)$.

The previous analysis was restricted to the assumption $\xi \ll 1$ which allowed us to apply a perturbation approximation. Next, we solve the steady IBL-model (26) numerically to (i) check the accuracy of the previous approximation and (ii) obtain solutions in parameter domains where $\xi = O(1)$. According to the assumption that the steady solution inherits the periodicity of the topography we apply periodic boundary conditions in the numerical procedure as well. A finite-difference scheme of second order is used to reduce Eq. (26) to a nonlinear algebraic equation which is solved with Newton's method.

Fig. 2 shows the free surface shape for different power-law indices n. We conclude that the free surface amplitude strongly depends on the power-law index n. For $n > 1$ the free surface amplitude is smaller than in the Newtonian case whereas it is higher for $n < 1$. Shear thinning liquids hence lead to an amplification of the free surface. It is obvious that a less 'viscous' liquid results in a stronger interaction of the free surface with the topography. The phenomenon of the surface amplification is called "resonance" in the literature (Wierschem et al., 2008; Heining et al., 2009) although it is not a dynamic process. At a particular Reynolds number the surface elevation forms a pronounced static hump which is fixed in space. Even though travelling waves are passing by this configuration remains steady. A detailed explanation of this phenomenon is given in Wierschem et al. (2008). First experimental evidence for resonance was provided by Vlachogiannis and Bontozoglou (2002) for rectangular corrugations and later by Wierschem and Aksel (2003) for sinusoidally corrugated topographies.

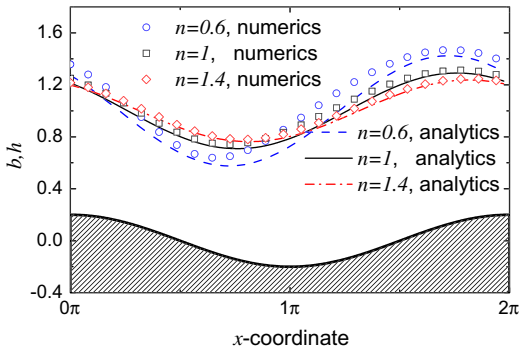

Fig. 2. Numerical and analytical free surface shapes. Lines indicate the analytical solution up to first order while the points indicate the numerical solution, respectively. The parameters are $\cot\alpha = 5$, $Bo^{-1} = 10$, Re = 40, $\delta = 0.2$, $\xi = 0.2$.

The comparison of the numerical results with the analytical approximation for the free surface shape in Fig. 2 shows that particularly, for $n = 1$ and $n = 1.4$ the solutions almost coincide. For $n = 0.6$ the numerical solution overestimates the analytical approximation. We suppose that this comes from the lacking contribution of the constant component which remains unaffected in the first order perturbation approximation, see Eq. (32).

In order to classify the free surface response at leading order we define the relative free surface amplitude and the relative film thickness amplitude by

$$a_h = \sqrt{S_1^2 + (1 + C_1)^2}, \quad a_f = \sqrt{S_1^2 + C_1^2}, \tag{33}$$

respectively. The relative free surface amplitude has the following physical interpretation: If for example $a_h = 1$ then the free surface amplitude has the same magnitude as the topography amplitude. The case $a_h > 1$ corresponds to an amplification, whereas $a_h < 1$ corresponds to a relative damping, compared to the topography amplitude. The same holds for the relative film thickness amplitude a_f. Next, we study the impact of the power-law index n on the relative film thickness amplitude a_f and the relative free surface amplitude a_h. The system depends on six parameters which are Re, δ, $\cot\alpha$, Bo^{-1}, ξ and n. In most of the following studies we fix $\delta = 0.2$, $\cot\alpha = 5$, $Bo^{-1} = 10$ to reduce the parameter space to a manageable set.

Fig. 3 depicts the amplitude of the free surface a_h and the film thickness a_f as a function of the Reynolds number. In both cases we observe that the amplitudes show a maximum, depending on n. The power-law index n has, as already predicted by Fig. 2, a strong influence on both amplitudes. Shear thickening liquids lead to decreased amplitudes in both cases, whereas shear thinning liquids lead to increased amplitudes. The position of the maximum is referred to as the resonant Reynolds number. For a_h the resonant Reynolds number decreases for decreasing n whereas the resonant Reynolds number for a_f hardly changes. The curves for a_h and a_f are both related to each other and have the same qualitative shape. In the following, we hence restrict our studies to the amplitude of the film thickness a_f.

We also compare the first harmonic of the numerical solution with the relative film thickness amplitude a_f of the perturbation approximation in Fig. 3b. Both solutions show a perfect agreement, independent of n. It hence can be concluded that the difference in Fig. 2 stems either from the constant component or higher harmonic contributions which are not part of the ansatz (30). The numerical solution is not restricted to monofrequent functions as assumed by the analytics but may in fact exhibit nonlinear higher harmonics.

The simple expression for a_f allows us to determine an expression for the resonant Reynolds number. We seek the position of the maximum by deriving a_f with respect to Re and computing the zero. A much easier approach, which yields the same result, can be found from the special form of a_f. Minimizing the denominator of S_1 and C_1 results in a maximum for a_f. We hence obtain for the resonant Reynolds number the simple expression

$$\mathrm{Re}_{res} = \frac{3(2+3n)}{2(1+2n)}\left(\frac{1}{3}\left(\frac{1+2n}{n}\right)^{n}\cot\alpha + Bo^{-1}\right), \tag{34}$$

where we have already resubstituted K_1 and K_2. In the Newtonian case with $n = 1$ Eq. (34) reduces to the known expression $\mathrm{Re}_{res,n=1} = \frac{5}{2}(\cot\alpha + Bo^{-1})$ from Heining et al. (2009). In the following, we study the impact of the power-law index n on the resonant Reynolds number (34). From (34) we conclude that high surface tension requires higher Reynolds numbers to achieve resonance. Inertial forces have to counteract the higher capillary pressure in this case. Shear thickening fluids also lead to an increase of the resonant Reynolds number since the increasing viscous forces have to be compensated by inertia. We also observe that the resonant Reynolds number increases with the cotangens of the inclination angle. As a consequence, resonance at lower inclination angles can only be obtained by increasing inertia.

Evaluating a_f at $\mathrm{Re} = \mathrm{Re}_{res}$ delivers an expression for the maximum relative amplitude which reads

$$a_{f\max} = \frac{1}{1+2n}\left(3\delta Bo\left(\frac{1+2n}{n}\right)^{-n} + \delta\cot\alpha\right). \tag{35}$$

In the Newtonian case Eq. (35) simplifies to $a_{f\max} = 1/3(\delta Bo + \delta\cot\alpha)$. We remark that decreasing n yields an increased maximum amplitude, independent of surface tension or inclination angle. As expected, shear thickening liquids lead to smaller amplitudes in

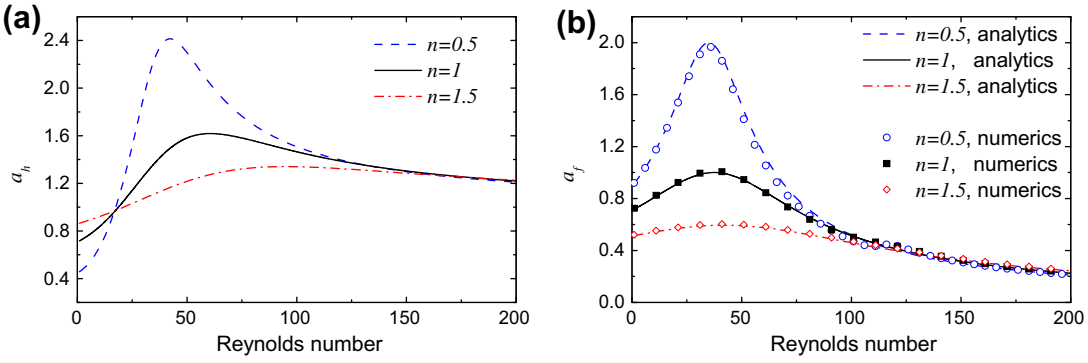

Fig. 3. Free surface a_h and film thickness amplitude a_f vs. Reynolds number. In plot (b) points indicate the numerical solution while lines indicate the analytical solution up to first order, respectively. The parameters are $Bo^{-1} = 10$, $\cot\alpha = 5$, $\delta = 0.2$.

both cases due to the increasing influence of viscous damping forces.

In the following, we focus on liquids which differ only slightly from the Newtonian case to highlight the influence of the power-law index n. We take the relative film thickness amplitude again as a measure for the free surface response and particularly consider the maximum value for $\mathrm{Re} = \mathrm{Re}_{res}$. The maximum amplitude $a_{f\max}$ is then expanded in a Taylor series around $n = 1$

$$a_{f\max} = \frac{1}{3}(\delta\cot\alpha + \delta Bo^{-1}) - a_{f\max_1}(n-1) + O((n-1)^2), \tag{36}$$

with the first order correction

$$a_{f\max_1} = \frac{(Bo^{-1}(1+3\ln 3) + 2\cot\alpha)}{9(Bo^{-1}+\cot\alpha)}(\delta Bo^{-1} + \delta\cot\alpha), \tag{37}$$

which is always positive. As a consequence, the maximal relative film thickness amplitude $a_{f\max}$ increases if $n < 1$ and decreases with $n > 1$. We hence confirm that a shear thinning liquid always leads to an increase of the maximum amplitudes due to a stronger interaction of the free surface with the topography.

The nonlinearity of the free surface is now studied by the Fourier decomposition of the film thickness. To this end, we increase the steepness parameter ξ further to reveal nonlinear effects. In Fig. 4 we plot the first four Fourier modes of the film thickness. It can be concluded that the order of magnitude decreases from order to order which yields an a posteriori confirmation of the ansatz (28) and (30). The second harmonic is of order $O(10^{-1})$ whereas the third is already of order $O(10^{-2})$. From Fig. 4a we conclude that the basic Fourier mode is not equal to 1 as assumed in the ansatz (28) but is larger. However, this effect decreases with increasing power-law index. This explains the deviation in Fig. 2 where the numerical solution overestimates the analytical approximation. Furthermore, the first harmonic in Fig. 4b based on the nonlinear theory shows in fact two maxima in contrast to the analytical result. We find another local maximum at higher Reynolds numbers which is further increased with decreasing power-law index n. Higher harmonics in (c) and (d) show a similar behaviour but the second maximum is even more pronounced. Both maxima seem to bend to the right with decreasing power-law index n. A similar effect has been observed by Heining et al. (2009) in the Newtonian case. They even found bistable resonance leading to a tilt of the resonance curve to the right.

4. Linear and nonlinear stability of the steady state

In the preceding section, we solved the integral boundary-layer model analytically for weak bottom amplitudes and numerically for higher bottom amplitudes. Next, we discuss the linear stability of the system. For this sake, we linearize the mass balance (22) and the IBL-model (25) around the steady state by substituting $(f,q) = (f_s(x),1) + \varepsilon(\tilde{f}(x,t),\tilde{q}(x,t))$ with $\varepsilon \ll 1$. The linearized equations at order ε^1 then read

$$\frac{\partial\tilde{h}}{\partial t} + \frac{\partial\tilde{q}}{\partial x} = 0, \tag{38}$$

and

$$\begin{aligned}\delta\mathrm{Re}\left(\frac{\partial\tilde{q}}{\partial t}f_S^3 + 2K_1\frac{\partial\tilde{q}}{\partial x}f_S^2 - K_1\frac{\partial\tilde{f}}{\partial x}f_S + (3K_1\tilde{f} - 2K_1q_1f_S)\frac{df_S}{dx}\right)\\ + 3\delta\cot\alpha K_2 f_S^4\frac{\partial\tilde{f}}{\partial x} - 3\delta Bo^{-1}f_S^4\frac{\partial^3\tilde{f}}{\partial x^3}\\ - \frac{1}{f_S^{2n-2}}K_2((6n+3)\tilde{f} - 3n\tilde{q}f_S) = 0,\end{aligned} \tag{39}$$

with the abbreviations K_1, K_2 introduced in (31). In (39) we already made use of the ε^0 – equation which has the consequence that (39) only depends on the steady solution $f_S(x)$ but not explicitly on the topography function $b(x)$. Introducing periodic perturbations of the form

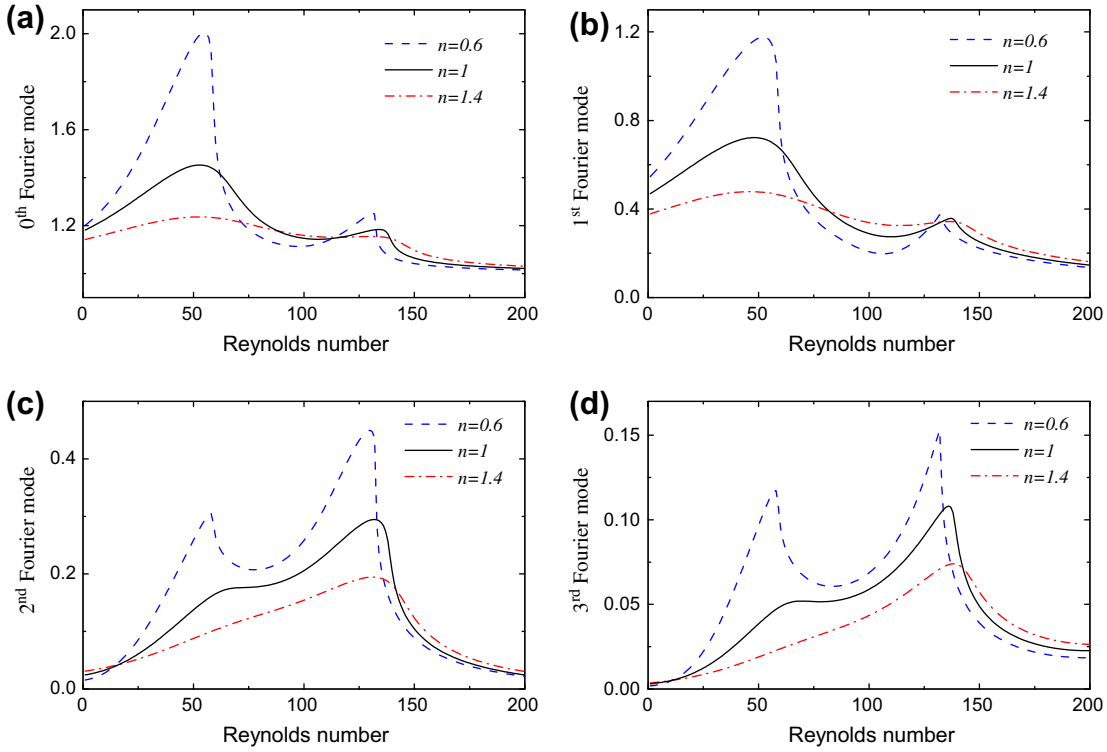

Fig. 4. The first four Fourier modes of the film thickness for the parameters $Bo^{-1} = 10$, $\cot\alpha = 5$, $\delta = 0.2$, $\xi = 0.6$.

$$\tilde{f} = \hat{f}(x)\exp(-i\omega t),\quad \tilde{q} = \hat{q}(x)\exp(-i\omega t), \tag{40}$$

where $\omega \in \mathbb{R}$ is the temporal frequency and $\hat{f}, \hat{q}$ are the amplitudes of the perturbation, yields

$$\begin{aligned} &-i\omega\hat{f} + \frac{d\hat{q}}{dx} = 0,\\ &\delta\mathrm{Re}\left(2K_1\frac{d\hat{q}}{dx}f_S^2 - K_1\frac{d\hat{f}}{dx}f_S - \hat{q}f_S^3\omega i - K_1(2\hat{q}f_S - 3\hat{f})\frac{df_S}{dx}\right)\\ &+3K_2\delta\cot\alpha\frac{d\hat{f}}{dx}f_S^4 - 3\delta Bo^{-1}\frac{d^3\hat{f}}{dx^3}f_S^4 - \frac{1}{f_S^{2n-2}}K_2((6n+3)\hat{f} - 3n\hat{q}f_S) = 0. \end{aligned} \tag{41}$$

In the following, we study the stability by prescribing the frequency of the perturbation ω and determining the corresponding amplitude functions $\hat{f}$ and $\hat{q}$ whose spatial evolution is responsible for the stability of the system. If $\hat{f}$ and $\hat{q}$ grow in space, the solution is unstable, otherwise it is stable, whereas the neutral case is given by spatially periodic amplitudes $\hat{f}$ and $\hat{q}$.

First, we rewrite (41) into a system of 4 ordinary differential equations of first order

$$\frac{d\mathbf{e}}{dx} = \mathbf{C}(x)\mathbf{e}(x), \tag{42}$$

where $(e_1, e_2, e_3, e_4) = (\hat{q}, d\hat{q}/dx, d^2\hat{q}/dx^2, d^3\hat{q}/dx^3)$. A detailed form of (42) is given in the Appendix. According to the periodicity of the steady system, the solution f_S and thus all coefficient functions of (41) are periodic with periodicity 2π. The same holds for the coefficient matrix $\mathbf{C}(x) \in \mathbb{C}^{4\times4}$, $\mathbf{C}(0) = \mathbf{C}(2\pi)$. The periodicity of the coefficients motivates us to apply monodromy theory (Jordan and Smith, 1987). The eigenvalues $\lambda_i, i = 1,\ldots,4$ of the monodromy matrix $\mathbf{M} = \mathbf{E}(2\pi)\mathbf{E}(0)^{-1}$ are responsible for stability or instability with $\mathbf{E}$ being the corresponding fundamental matrix. The solution can then be written as $\mathbf{e}_i = \mathbf{e}_i^0(x)\exp(\rho_i x)$ where ρ_i are the Floquet exponents with $\exp(2\pi\rho_i) = \lambda_i$ and $\mathbf{e}_i^0(x)$ are periodic functions, respectively. Since $\mathbf{e}_i^0(x)$ are periodic they have no influence on the stability and thus stability is only governed by the eigenvalues λ_i. If $|\lambda_i| < 1, i = 1,\ldots4$, then the solution is stable, otherwise, it is unstable. In the limit case $|\lambda_i| = 1, i = 1,\ldots4$ the solution for $\mathbf{e}$ and thus for $\hat{f}$ and $\hat{q}$ is periodic.

We determine the eigenvalues of $\mathbf{M}$ for varying Re and ω. The matrix $\mathbf{M}$ and the eigenvalues λ_i are computed numerically. As a first test example we consider the known case of a Newtonian liquid flowing down an inclined flat plane. The critical Reynolds number for instability reads $\mathrm{Re}_{crit} = \cot\alpha$. It has to be noted that the critical Reynolds number determined by the integral boundary-layer model differs by a factor 5/6 from the exact value (Yih, 1963). Ruyer-Quil and Manneville (2000) developed a weighted-residual integral boundary-layer model which was recently extended by Oron and Heining (2008) to the Newtonian flow over an undulated incline both predicting the correct critical Reynolds number $\mathrm{Re}_{crit} = (5/6)\cot\alpha$ for the flat incline. However, the derivation of the extended equations is highly complicated; nevertheless the qualitative behaviour is identical and the gain has only minor quantitative impact.

From the numerical studies in the well known case $\xi = 0$ and $n = 1$ we conclude that three of the four independent solutions are physically not realistic since the corresponding eigenvalues are either always stable or always unstable. We hence focus on the physically realistic eigenvalue which correctly reproduces the limit case $\xi = 0$ and $n = 1$. For the non-Newtonian case with $n \neq 1$ but $\xi = 0$ the corresponding critical Reynolds number $\mathrm{Re}_{crit} = (1+2n)^{n-1}n^{2-n}\cot\alpha$ confirms the results given in Dandapat and Mukhopadhyay (2001). The neutral curve reads

$$\mathrm{Re} = (1+2n)^{n-1}n^{2-n}\cot\alpha + (3Bo^{-1}n^4(1+2n)^{-3})\omega^2. \tag{43}$$

Considering (43) we find out that increasing the power-law index n leads to an increase of the critical Reynolds number, while decreasing n decreases the domain of stability. It is obvious that a less 'viscous' fluid becomes unstable at lower Reynolds numbers. The critical Reynolds number lies at $\omega = 0$ which is an indicator for the long-wave instability of the system.

In the following, we use the known case (43) as a starting point and discuss the dependence of the neutral curve and the critical Reynolds number on the steepness parameter ξ. Fig. 5 shows curves for Newtonian (a), shear thickening (b) and shear thinning (c) fluids. From the case in (a) we conclude that the neutral curves are shifted to the right with increasing bottom steepness. Furthermore, the neutral curves exhibit a dent for higher ξ which finally leads to the separation of the neutral curve into two disjoint domains. The character of the instability is still long-wave, however, the critical Reynolds number increases which yields a stabilizing with increasing ξ. For shear thickening fluids in case (b) the stabilizing is even more pronounced. Furthermore, the dent grows which finally yields a neutral curve which is located at the upper right. As a consequence, the system is unstable with respect to a short-wave instability. A completely different configuration concerning the critical Reynolds number is obtained in the shear thinning case (c). For small ω the neutral curves are shifted to smaller Reynolds numbers which corresponds to a destabilizing of the system. At higher steepness parameters the neutral curve shows a dent and another stable domain at higher Reynolds numbers.

We conclude that a stabilizing or destabilizing effect of the topography strongly depends on the power-law index n. This motivates us to focus on the critical Reynolds number as a function of the power-law index n and the steepness parameter ξ. Since the critical Reynolds number depends on n as well, we consider the ratio of the critical Reynolds number for the flow over an undulated topography to the critical Reynolds number for the flow over a flat incline in order to highlight the impact of the undulation. We therefore define

$$\zeta = \frac{\mathrm{Re}_{crit}(\xi, n)}{\mathrm{Re}_{crit}(0, n)}, \tag{44}$$

which measures the stabilizing or destabilizing as a function of the steepness parameter. The factor ζ is referred to as the stabilization factor in the following. If $\zeta > 1$ the topography has a stabilizing influence, if $\zeta < 1$ it has a destabilizing influence, compared to the flow over a flat incline.

Fig. 6 depicts the stabilization factor for increasing ξ. We confirm the assumptions we already made with the help of Fig. 5: Increasing the steepness parameter leads to a stabilizing effect for $n > 1$. The stabilizing almost reaches a factor 3 which corresponds to a critical Reynolds number which is three times larger than that of the corresponding flat incline. For larger steepness parameters ξ the stabilizing effect weakens and the factor ζ decreases again for higher values of ξ. For shear thinning fluids with $n < 1$ the effects are different. In the cases $n = 0.8$ and $n = 0.9$ we observe that the undulation has a destabilizing influence on the flow. For $n = 0.8$ and $\xi = 0.5$ the critical Reynolds number is only half of that of the flow over a flat incline. We note that similar curves of critical Reynolds numbers have already been observed by D'Alessio et al. (2009) in the Newtonian case by studying a weighted-residual integral boundary-layer model of higher order. Heining and Aksel (2009) found qualitatively similar effects for the corresponding inverse problem.

The linear stability maps will now be completed by a full nonlinear study. The aims of this approach is twofold: (i) To draw the neutral curves more precisely and (ii) to clarify the existence of the peninsulas and islands in the stability maps in Fig. 5. To this

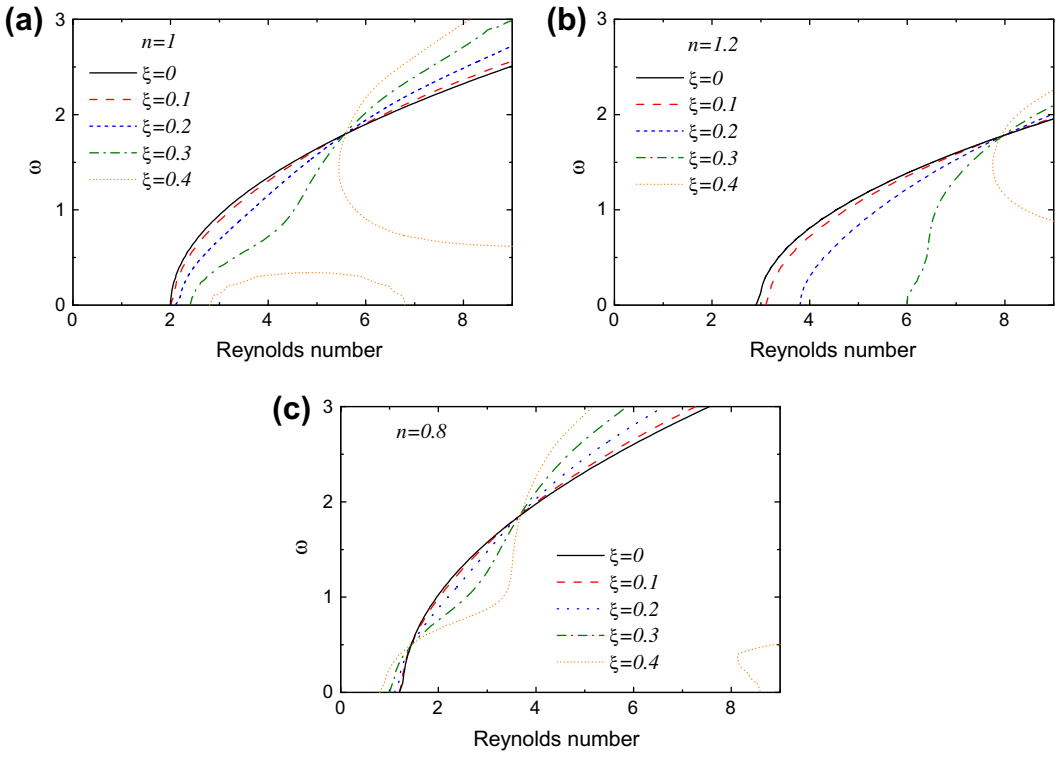

Fig. 5. Neutral curves for varying bottom steepnesses ξ and different power-law indices n. (a) $n = 1$, (b) $n = 1.2$ and (c) $n = 0.8$. The other parameters are $\cot\alpha = 2$, $\delta = 0.3$, $Bo^{-1} = 10$.

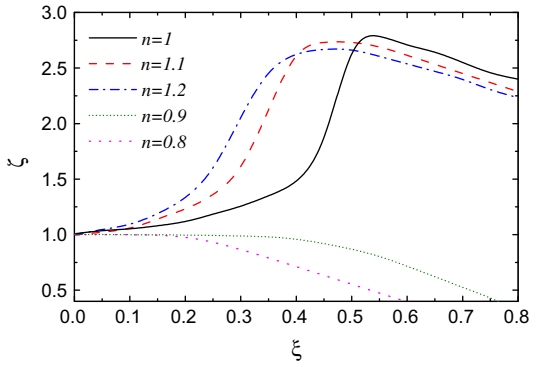

Fig. 6. Stabilization factor ζ as a function of the steepness parameter ξ. The parameters are $Bo^{-1} = 10$, $\cot\alpha = 2$, $\delta = 0.3$.

end, we solve the full time-dependent integral boundary-layer model (22), (25) numerically.

In contrast to the steady solution where we assumed periodicity in spatial direction, an open flow domain is now necessary. Furthermore, we have to define an initial condition which is set to $q(x, t = 0) = 1, f(x, t = 0) = 1$. The inlet boundary condition is given by a time-periodic perturbation with frequency ω. We prescribe the flow rate at $x = 0$ by assuming $q = 1 + \tilde{\varepsilon}\sin(\omega t)$ with $\tilde{\varepsilon} = 0.2$. At the exit the outlet boundary condition has to be as neutral as possible to avoid reflections in the upstream direction. On the other hand, the convective character of the system with a dominant main flow direction has the consequence that only a small fraction of the entire channel is affected by perturbations due to the exit condition. We find that a fixed film thickness and a fixed flow rate at the outflow results in small reflections upstream. Furthermore, we neglect the lowest part of the channel and only consider the numerical solution in the upper part to ensure no influence of the outlet. Since the stability of the flow is of interest we also have to extend the solution domain to several periods of the topography. Typically, we use 300 periods of the topography as the solution domain and determine whether the perturbations coming from the inlet are damped or amplified. This yields for every pair of Reynolds numbers and excitation frequencies a criterion for stability or instability. The IBL-model itself is solved using a finite-difference scheme. The derivatives in spatial direction are approximated using first order difference quotients. Next, the resulting system of ordinary differential equations is solved with a second order Runge–Kutta method.

The results of the nonlinear analysis are shown in Fig. 7 where we display the neutral curves in comparison with the linear analysis. First, the qualitative agreement is perfect even for higher Reynolds numbers. Second, we find that the nonlinear analysis does not confirm the appearance of the peninsula in Fig. 7a. Also the lower branch of the neutral curve for $\xi = 0.4$ in Fig. 7b is not recovered. Thus, their existence does not reflect the physical reality but must be attributed to the weakness of the linearization.

5. The role of capillarity

The thin-film approach of the previous sections is applicable in the case of moderate inverse Bond numbers with $\delta Bo^{-1} = 1$. From the parameter studies concerning the steady state and the resonance we conclude that the inverse Bond number has a strong influence on (i) the resonant Reynolds number and (ii) the amplitude for resonance. Furthermore, surface tension contributes to the governing equation (25) together with the highest derivative which highlights its special role. This motivates further parameter studies for smaller surface tension coefficients.

To begin with, we consider the resonance cases in Fig. 4 and determine the Fourier decomposition of the film thickness for smaller inverse Bond numbers keeping all the other parameters

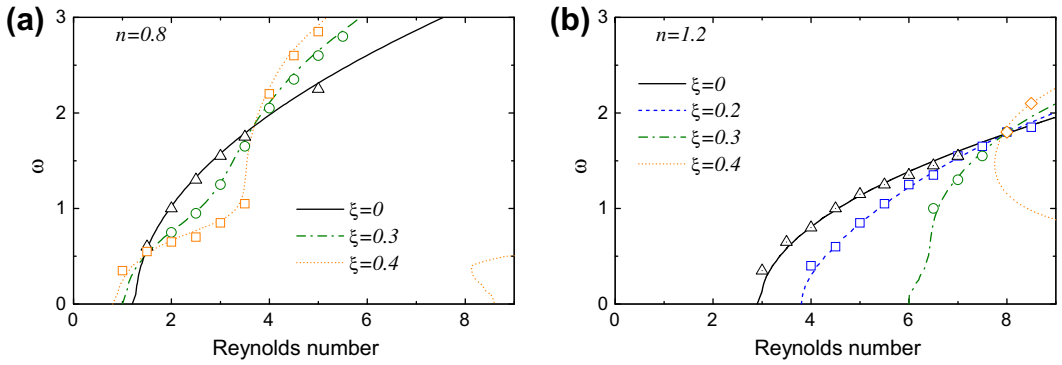

Fig. 7. Comparison of the linear and nonlinear neutral curves. (a) $n = 0.8$, (b) $n = 1.2$. Lines indicate the results of the linear and symbols indicate the results of the nonlinear analysis, respectively. The parameters are $\cot\alpha = 2$, $\delta = 0.3$, $Bo^{-1} = 10$.

fixed. The results are depicted in Fig. 8. We find that (i) It is obvious that for the zeroth and the first Fourier mode the second maximum disappears completely while the second maximum for higher Fourier modes only occurs for smaller values of the power-law index n. (ii) The maxima are much smaller and consequently the resonance is weaker. It can be concluded that the steady solution is significantly influenced by the surface tension.

Further surface tension effects become obvious in the stability problem. For the non-Newtonian flow over a flat incline the critical Reynolds number reads $\mathrm{Re}_{crit} = (1+2n)^{n-1} n^{2-n} \cot\alpha$. It is clear that increasing n and increasing $\cot\alpha$ lead to an increasing critical Reynolds number which is independent of the surface tension. For a flat incline where the steady solution yields a flat free surface, surface tension plays a secondary role. However, in the case of an undulated topography, where the base solution has already a curved shape the influence of surface tension grows in importance. The results of the previous sections show that the impact of a periodic topography on the stability depends on the power-law index n. Compared to the flow over a flat incline both, stabilizing or destabilizing effects are possible.

In the following, we point out the influence of surface tension on the neutral curves and on the critical Reynolds number. Fig. 9 shows neutral curves for the same parameters as in Fig. 5 but with smaller inverse Bond numbers. A completely different qualitative behaviour is evident. First, we observe no indentations, no formation of islands or peninsulas in the stability map and secondly the topography yields for both cases, shear thinning and shear thickening, a stabilizing compared to the corresponding flow over a flat incline. We hence assume that the effects in Fig. 5 mainly arise from high values of surface tension. For smaller or moderate surface tension coefficients the neutral curves are only shifted to the right without strong changes in shape.

It has to be noted that a destabilizing effect of a periodic topography on a Newtonian flow has already been reported in literature (Heining and Aksel, 2009; D'Alessio et al., 2009; Häcker and Uecker, 2009). However, a destabilizing effect arises only – in line with

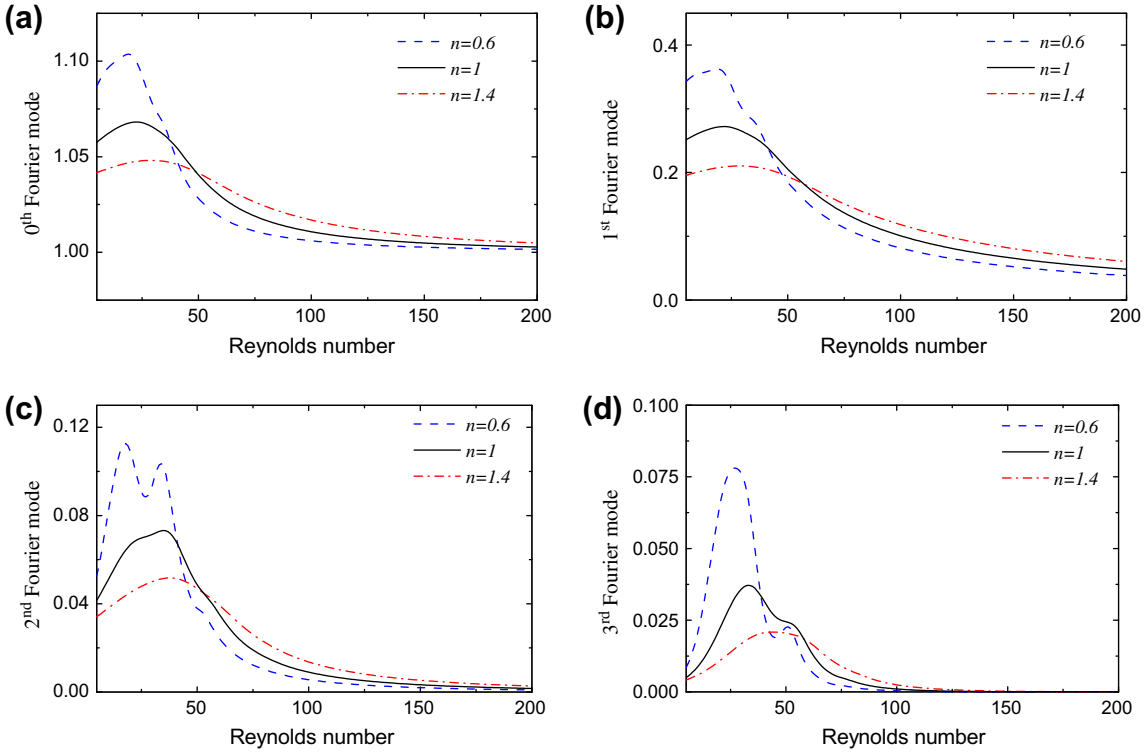

Fig. 8. The first four Fourier modes of the film thickness for the parameters $Bo^{-1} = 1$, $\cot\alpha = 5$, $\delta = 0.2$, $\xi = 0.6$.

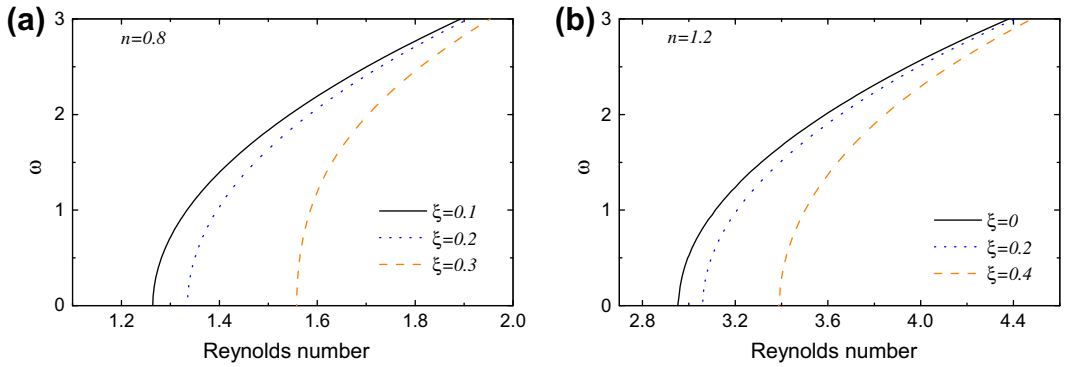

Fig. 9. Neutral curves for varying steepnesses parameter ξ and different power-law indices n. (a) $n = 0.8$, (b) $n = 1.2$ and. The other parameters are $\cot\alpha = 2$, $\delta = 0.3$, $Bo^{-1} = 1$.

the present work – if surface tension is strong enough. For smaller surface tensions, the topography always yields a stabilizing effect, which has been already confirmed experimentally (Vlachogiannis and Bontozoglou, 2002; Wierschem et al., 2005; Argyriadi et al., 2006) and theoretically (Wierschem and Aksel, 2003; Dávalos-Orozco, 2007, 2008; Trifonov, 2007a,b). The influence of the topography on the stability of thin films for higher inverse Bond numbers has not been reported experimentally yet.

6. Discussion

We have found that the power-law index has a significant influence on the steady surface deformation of a film over an undulated topography. While shear-thickening flows lead to a decrease, shear thinning flows lead to an amplification of the steady free surface. This resonance-like phenomenon is further studied by considering the first Fourier modes of the film thickness as a measure for the free surface amplification. We find that for increasing Reynolds number the amplitudes show two maxima, indicating high surface deformations. Shear thinning fluids even amplify this effect. However, in the case of smaller surface tension, viscous effects are dominant which lead to a smoothening of the free surface and decreased free surface amplitudes.

Although the Reynolds numbers in the studied regime are quite high which implies unsteady motion we nevertheless consider the flow in a steady framework. A justification of this lies in the convective character of the system which has the consequence that possible perturbations travel downstream and affect the steady solution only temporarily. Further deeper arguments and experimental validations can be found in Wierschem et al. (2008), Vlachogiannis and Bontozoglou (2002), Wierschem and Aksel (2004a).

The steady investigation is complemented by a stability analysis. It is shown how the shear thinning or shear thickening properties and the topography affect the stability of the system. A linear stability analysis reveals that several qualitatively different effects are possible. Increasing the steepness of the topography we find that the flow is stabilized for shear thickening fluids. For shear thinning fluids the topography leads to a destabilization, always compared to the case of the flow over a flat incline. Furthermore, the stability maps show disjoint unstable islands for increasing steepness. A nonlinear stability analysis provides further insight into the stability of the system. Most of the neutral curves show a perfect agreement with the nonlinear stability analysis. However, we find that the formation of disjoint unstable islands cannot be reproduced by the nonlinear simulations and hence must be attributed to the linearization.

A study on the inverse Bond number reveals that surface tension has a significant impact on the stability of the film. While for higher surface tensions both regimes, a stabilization and a destabilization depending on the power-law index are possible, the effect changes qualitatively for smaller surface tension coefficients. For smaller inverse Bond numbers the undulated topography always leads to a stabilization, independent of the power-law index. The destabilization of thin film flows at high inverse Bond numbers has not been reported experimentally yet.

Appendix A. Derivation of the system (42)

To begin with, we eliminate $\hat{f}$ from Eq. (41) to obtain a single fourth order equation for $\hat{q}$ only. We then obtain

$$\delta\mathrm{Re}\left(2K_1 i\omega\frac{d\hat{q}}{dx}f_S^2 - K_1\frac{d^2\hat{q}}{dx^2}f_S + \hat{q}f_S^3\omega^2 - \left(2K_1\hat{q}i\omega f_S - 3K_1\frac{d\hat{q}}{dx}\right)\frac{df_S}{dx}\right) + 3K_2\delta\cot\alpha\frac{d^2\hat{q}}{dx^2}f_S^4 - 3\delta Bo^{-1}\frac{d^4\hat{q}}{dx^4}f_S^4 - \frac{1}{f_S^{2n-2}}K_2\left(6n\frac{d\hat{q}}{dx} - 3in\hat{q}f_S\omega + 3\frac{d\hat{q}}{dx}\right) = 0. \tag{45}$$

Rewriting Eq. (45) into a system with $d\mathbf{e}/dx = \mathbf{C}(x)\mathbf{e}(x)$ and the vector $(e_1, e_2, e_3, e_4) = (\hat{q}, \frac{d\hat{q}}{dx}, \frac{d^2\hat{q}}{dx^2}, \frac{d^3\hat{q}}{dx^3})$ yields the coefficient matrix

$$\mathbf{C}(x) = \begin{pmatrix} 0 & 1 & 0 & 0 \\ 0 & 0 & 1 & 0 \\ 0 & 0 & 0 & 1 \\ C_{41} & C_{42} & C_{43} & 0 \end{pmatrix}, \tag{46}$$

where we introduced the matrix entries

$$\begin{aligned} C_{41} &= \frac{1}{3\delta Bo^{-1}f_S^4}\left[\delta\mathrm{Re}\left(f_S^3\omega^2 - 2K_1 i\omega f_S\frac{df_S}{dx}\right) + 3\frac{nK_2}{f_S^{2n-2}}i\omega f_S\right], \\ C_{42} &= \frac{1}{3\delta Bo^{-1}f_S^4}\left[\delta\mathrm{Re}\left(2K_1 i\omega f_S^2 + 3K_1\frac{df_S}{dx}\right) - \frac{(6n+3)K_2}{f_S^{2n-2}}\right], \\ C_{43} &= \frac{1}{3\delta Bo^{-1}f_S^4}\left[-\delta\mathrm{Re}K_1 f_S + 3K_2\delta\cot\alpha f_S^4\right], \end{aligned} \tag{47}$$

References

Aksel, N., Heymann, L., 2007. Rheology of emulsions and suspensions. In: Tropea, C., Yarin, A.L., Foss, J.F. (Eds.), Handbook of Experimental Fluid Mechanics. Springer, Berlin, pp. 680–720.

Amaouche, M., Djema, A., Bourdache, L., 2009. A modified Shkadov's model for thin film flow of a power-law fluid over an inclined surface. C. R. Mecanique 337, 48–52.

Argyriadi, K., Vlachogiannis, M., Bontozoglou, V., 2006. Experimental study of inclined film flow along periodic corrugations: the effect of wall steepness. Phys. Fluids 18, 012102.

Berezin, A.Yu., Hutter, K., Spodareva, L.A., 1998. Stability analysis of gravity driven shear flow with free surface for power-law fluids. Arch. Appl. Mech. 68, 169–178.
Craster, R.V., Matar, O.K., 2009. Dynamics and stability of thin liquid films. Rev. Mod. Phys. 81, 1131–1198.
D'Alessio, S.J.D., Pascal, J.P., Jasmine, H.A., 2009. Instability in gravity-driven flow over uneven surfaces. Phys. Fluids 21, 062105.
Dandapat, B.S., Mukhopadhyay, A., 2001. Waves on a film of power-law fluid flowing down an inclined plane at moderate Reynolds number. Fluid Dyn. Res. 29, 199–220.
Dandapat, B.S., Mukhopadhyay, A., 2003. Waves on the surface of a falling power-law fluid film. Int. J. Non-Linear Mechanics 38, 21–38.
Dávalos-Orozco, L.A., 2007. Nonlinear instability of a thin film flowing down a smoothly deformed surface. Phys. Fluids 19, 074103.
Dávalos-Orozco, L.A., 2008. Instabilities of thin films flowing down flat and smoothly deformed walls. Microgravity Sci. Technol. 20, 225–229.
Fernandez, P., Heymann, L., Ott, A., Aksel, N., Pullarkat, P.A., 2007. Shear rheology of a cell monolayer. New J. Phys. 9, 419.
Fowler, A.C., 1982. Waves on glaciers. J. Fluid Mech. 120, 283–321.
Gaskell, P.H., Jimack, P.K., Sellier, M., Thompson, H.M., 2006. Flow of evaporating, gravity-driven thin liquid films over topography. Phys. Fluids 18, 013601.
Gupta, A.S., 1967. Stability of a visco-elastic liquid film flowing down an inclined plane. J. Fluid Mech. 28, 17–28.
Häcker, T., Uecker, H., 2009. An integral boundary layer equation for film flow over inclined wavy bottoms. Phys. Fluids 21, 092105.
Heining, C., Aksel, N., 2009. Bottom reconstruction in thin-film flow over topography: steady solution and linear stability. Phys. Fluids 21, 083605.
Heining, C., Bontozoglou, V., Aksel, N., Wierschem, A., 2009. Nonlinear resonance in viscous films on inclined wavy planes. Int. J. Multiphase Flow 35, 78–90.
Hutter, K., Svendsen, B., Rickenmann, D., 1996. Debris flow modeling: a review. Continuum Mech. Thermodyn. 8, 1–35.
Jordan, D.W., Smith, P., 1987. Nonlinear Ordinary Differential Equations, second ed. Oxford University Press.
Kanaris, A.G., Mouza, A.A., 2006. Flow and heat transfer prediction in a corrugated plate heat exchanger using a CFD code. Chem. Eng. Technol. 29, 923–930.
Kármán, Th.v., 1921. Über laminare und turbulente Reibung. ZAMM 1, 233–252.
Kistler, S.F., Schweizer, P.M., 1997. Liquid Film Coating. Chapman & Hall, New York.
Lawrence, C.J., Zhou, W., 1991. Spin coating of non-Newtonian fluids. J. Non-Newtonian Fluid Mech. 39, 137–187.
Luo, H.X., Pozrikidis, C., 2007. Gravity-driven film flow down an inclined wall with three-dimensional corrugations. Acta Mech. 188, 209–225.
Miladinova, S., Lebon, G., Toshev, E., 2004. Thin-film flow of a power-law liquid falling down an inclined plate. J. Non-Newtonian Fluid Mech. 122, 69–78.
Oron, A., Heining, C., 2008. Weighted-residual integral boundary-layer model for the nonlinear dynamics of thin liquid films falling on an undulating vertical wall. Phys. Fluids 20, 082102.
Pascal, J.P., 2003. A two-layer model for a non-Newtonian gravity current subjected to wind shear. Acta Mech. 162, 83–98.
Pascal, J.P., 2006. Instability of power-law fluid down a porous incline. J. Non-Newtonian Fluid Mech. 133, 109–120.
Pascal, J.P., D'Alessio, S.J.D., 2007. Instability of power-law fluid flows down an incline subjected to wind stress. Appl. Math. Model. 31, 1229–1248.
Pascal, J.P., D'Alessio, S.J.D., 2010. Instability in gravity-driven flow over uneven permeable surfaces. Int. J. Multiphase Flow 36, 449–459 .
Pohlhausen, K., 1921. Zur näherungsweisen Integration der Differentialgleichung der laminaren Reibungsschicht. ZAMM 1, 252–268.
Pozrikidis, C., 2003. Effect of surfactants on film flow down a periodic wall. J. Fluid Mech. 496, 105–127.
Ruyer-Quil, C., Manneville, P., 2000. Improved modelling of flows down inclined planes. Eur. Phys. J. B 15, 357–369.
Sadiq, I.M.R., Usha, R., 2008. Thin Newtonian film flow down a porous inclined plane: Stability analysis. Phys. Fluids 20, 022105.
Saprykin, S., Koopmans, R.J., Kalliadasis, S., 2007. Free-surface thin-film flows over topography: influence of inertia and viscoelasticity. J. Fluid Mech. 578, 271–293.
Scholle, M., Wierschem, A., Aksel, N., 2004. Creeping films with vortices over strongly undulated bottoms. Acta Mech. 168, 167–193.
Scholle, M., Haas, A., Aksel, N., Wilson, M.C.T., Thompson, H.M., Gaskell, P.H., 2009. Competing geometric and inertial effects on local flow structure in thick gravity-driven fluid films. Phys. Fluids 20, 123101.
Shkadov, V.Ya., 1967. Wave regimes of thin layer flow of viscous fluid under the gravity effect. Izv. AN SSR. Mekh. Zhidk Gaza 1, 43–51.
Spurk, J.H., Aksel, N., 2008. Fluid Mechanics, second ed. Springer, Berlin.
Teipel, U., Heymann, L., Aksel, N., 2001. An experimental study on the flow behaviour of micellar solutions. Exp. Fluids 30, 584–591.
Trifonov, Y.Y., 1998. Viscous liquid film flows over a periodic surface. Int. J. Multiphase Flow 24, 1139–1161.
Trifonov, Y.Y., 2007a. Stability and nonlinear wavy regimes in downward film flows on a corrugated surface. J. Appl. Mech. Tech. Phys. 48, 91–100.
Trifonov, Y.Y., 2007b. Stability of a viscous liquid film flowing down a periodic surface. Int. J. Multiphase Flow 33, 1186–1204.
Tseluiko, D., Blyth, M.G., Papageorgiou, D.T., Vanden-Broeck, J.-M., 2008. Electrified viscous thin film flow over topography. J. Fluid Mech. 597, 449–475.
Vlachogiannis, M., Bontozoglou, V., 2002. Experiments on laminar film flow along a periodic wall. J. Fluid Mech. 457, 133–156.
Wierschem, A., Aksel, N., 2003. Instability of a liquid film flowing down an inclined wavy plane. Physica D 186, 221–237.
Wierschem, A., Aksel, N., 2004a. Hydraulic jumps and standing waves in gravity-driven flows of viscous liquids in wavy open channels. Phys. Fluids 16, 3868–3877.
Wierschem, A., Aksel, N., 2004b. Influence of inertia on eddies created in films creeping over strongly undulated substrates. Phys. Fluids 16, 4566–4574.
Wierschem, A., Scholle, M., Aksel, N., 2002. Comparison of different theoretical approaches to experiments on film flow down an inclined wavy channel. Exp. Fluids 33, 429–442.
Wierschem, A., Scholle, M., Aksel, N., 2003. Vortices in film flow over strongly undulated bottom profiles at low Reynolds numbers. Phys. Fluids 15, 426–435.
Wierschem, A., Lepski, C., Aksel, N., 2005. Effect of long undulated bottoms on thin gravity-driven films. Acta Mech. 179, 41–66.
Wierschem, A., Bontozoglou, V., Heining, C., Uecker, H., Aksel, N., 2008. Linear resonance in viscous films on inclined wavy planes. Int. J. Multiphase Flow 34, 580–590.
Yih, C.S., 1963. Stability of liquid flow down an inclined plane. Phys. Fluids 6, 321–334.